Asymmetric tri-block copolymer nanocarriers for controlled localization, and pH sensitive release of proteins

Journal:	*Langmuir*
Manuscript ID	la-2016-01803t.R2
Manuscript Type:	Article
Date Submitted by the Author:	05-Sep-2016
Complete List of Authors:	Vasquez, Daniela; Universidad de Carabobo, Einfalt, Tomaz; University Basel, Chemistry Department Meier, Wolfgang; University of Basel, Department of Chemistry Palivan, Cornelia; University of Basel, Chemistry Department

Asymmetric tri-block copolymer nanocarriers for controlled localization, and pH sensitive release of proteins

Daniela Vasquez[†⊥], *Tomaz Einfalt*[†⊥], *Wolfgang Meier*[†], *Cornelia G. Palivan*[†*]

[†]*Department of Chemistry, University of Basel, Klingelbergstrasse 80 CH-4056 Basel, Switzerland*

ABSTRACT

Designing nanocarriers to release proteins under specific conditions is required to improve therapeutic approaches, especially in treating cancer and protein deficiency diseases. We present here supramolecular assemblies based on asymmetric poly(ethylengycol)-*b*-poly(methylcaprolactone)-*b*-poly(2-(*N*,*N*diethylamino)ethylmethacrylate) (PEG-*b*-PMCL-*b*-PDMAEMA) copolymers for controlled localization, and pH-sensitive release of proteins. Copolymers self-assembled in soft nanoparticles with a core domain formed by PMCL, and a hydrophilic domain based on PEG mainly embedded inside, and the branched PDMAEMA exposed at the particle surface. We selected as model proteins to be attached to the nanoparticles bovine serum albumin (BSA), and acid sphingomyelinase (ASM), the latter being an ideal

candidate for protein replacement therapy. The hydrophilic/hydrophobic ratio, nanoparticle size, and the nature of biomolecules are key factors for modulating protein localization and attachment efficiency. The predominant outer shell of PDMAEMA allows efficient pH-triggered release of BSA and ASM, and in acidic conditions >70% of the bound proteins were released. Up-take of protein-attached nanoparticles by HELA cells, together with low toxicity and pH responsive release, support such protein-bound nanoparticles as efficient stimuli-responsive candidates for protein therapy.

INTRODUCTION

Protein therapy, one of the most effective treatments for several diseases, aims to increase the levels of proteins that are deficient, displace dysfunctional proteins, deliver functional proteins into the cells, or inhibit a biological process by a specific protein.[1] However, direct administration of proteins is often ineffective because of low bioavailability, rapid degradation, and low permeability through membranes.[2] The need to develop novel solutions for these problems has led to the design of carriers with sizes in nanometer range for efficient transport and delivery in specific spatial and time conditions. In particular, a large variety of polymer 3D assemblies (particles, capsules, micelles, or vesicles) in which specific proteins are entrapped, encapsulated or attached have been introduced recently.[3] Protein entrapment depends on the chemical nature of the copolymer, its molecular weight, the presence of end groups, and protein-polymer interactions.[4] By selecting the components of the supramolecular assembly, and the site of internal protein localization,[5] controlled protein release is possible as a result of changes in protein-polymer interactions.[5,6] In this respect, copolymer assemblies based on PCL-PEG-PCL[7,8], PEO-PCL-PAA[9] and PEG-PCL-PAA[10] have been used to study their interactions with

model proteins, such as bovine serum albumin (BSA). Of particular interest are supramolecular assemblies that are responsive to various stimuli, such as pH, temperature or the presence of chemical or biological compounds.[11] Such assemblies allow the release of proteins in the presence of a stimulus, either by degradation of the assembly or by detachment of the biomolecules induced by a change in protein-polymer interactions.[11] For example, pH responsive assemblies have high potential for medical applications because pH is an essential signaling factor that accompanies pathological conditions (e.g. inflammation, cancerous tissue).[12] Various pH responsive polymer assemblies such as polyionic complex micelles,[13] nanocapsules,[14] or aldehyde displaying silica nanoparticles[15] have been used to deliver therapeutic drugs. In particular, PEG-*b*-PCL-*b*-PDMAEMA assemblies have been reported as delivery carriers for RNA[16], DNA[17] and SiRNA,[9] but not yet for proteins.

Here we present nanoparticles based on PEG-*b*-PMCL-*b*-PDMAEMA asymmetric copolymers for controlled localization and subsequent pH-sensitive release of proteins. We have evaluated the efficacy both with a model protein, bovine serum albumin fluorescein isothiocyanate conjugate (BSA-FITC), and acid sphingomyelinase (ASM), known for its role in catalyzing the breakdown of sphingomyelin to ceramide in the treatment of Niemann-Pick disease.[18] ASM entrapment in polymer nanoparticles with controlled localization and pH-responsive release represents a more appropriate solution for this pathology compared to the previous entrapment in non-responsive PLGA nanoparticles.[19] We have selected asymmetric tri-block copolymers PEG-*b*-PMCL-*b*-PDMAEMA to self-assemble into nanoparticles that support a specific localization for the proteins, and benefit from their biocompatibility and biodegradability.[20] The presence of the PDMAEMA block induces pH responsiveness, whilst poly(methylcaprolactone) (PMCL) favors the formation of more stable 3D assemblies, because it is fluid at room temperature, and

more hydrophobic than (poly caprolactone) PCL due to the presence of the methyl groups.[21] The formation and stability of the polymer nanoparticles in buffer, as relevant environment for attachment of proteins, have been characterized by a combination of light scattering, transmission electron microscopy (TEM and cryo-TEM), and fluorescence correlation spectroscopy (FCS). The effect of the ratio between the hydrophobic block and the pH-sensitive block on the entrapment/release of ASM allowed improvements in the system efficiency for protein delivery. Activity assays were performed to establish whether protein entrapment affected its activity once released from the nanoparticles, whilst up-take and toxicity in HeLa cells were evaluated by a combination of [3-(4,5-dimethylthiazol-2-yl)-5-(3-carboxymethoxyphenyl)-2-(4-sulfophenyl)-2H-tetrazolium (MTS) assay and fluorescence activated cell sorting (FACS). To the best of our knowledge, our study is the first one focussed on a pH responsive proteins delivery by nanoparticles resulting from the smart use of an asymmetric triblock copolymer, which serves to direct protein localization in the architecture of the nanoparticles. Our stimuli-responsive nanoparticles with controlled localization of proteins represent a smart solution for protein therapy, serving to improve the release as a key parameter for efficient therapeutic solutions.

EXPERIMENTAL SECTION

Materials and methods Poly(ethyleneglycol) monomethylether (mPEG) with molar mass of 2000 Da and 2-(dimethylamino)ethyl methacrylate were obtained from Sigma Aldrich. Monomer methacrylate was prepared by using 4-methylcyclohexanone and m-chloroperoxy-benzoic acid also purchased from Sigma Aldrich. The bovine serum albumin (BSA) (M_w = 66 KDa; I.P: 4.7 at

25°C in PBS), BSA conjugated with fluorescein isothiocyanate (BSA-FITC, labelling efficiency 11-12 mol FTIC / 1 mol BSA) and acid sphingomyelinase from Acid Sphinomyelinase (ASM) (M_w = 67 KDa; I.P: 6.8 at 25°C in PBS) were purchased from Sigma Aldrich and all the solvents for self-assembly (ethanol and PBS buffer) were used without further purification.

Synthesis of mPEG-b-PMCL-PDMAEMA triblock copolymers

mPEG-b-PMCL-PDMAEMA triblock copolymers were synthesized according to the procedure described by Matter et al. [20], by using poly (ethyleneglycol) monomethylether (mPEG) with a molar mass of 2000 Da (Aldrich), copper (I) chloride (Reagent plus > 99 %, Sigma Aldrich), N, N, N′, N″, N″-pentamethyldiethylenetriamine (PMDETA) (> 99%, Aldrich), THF (Fluka), methanol, 2-bromoisobutyrylbromide (BIBB > 98%, Sigma Aldrich), triethylamine (> 99.5%, Fluka) and dichloromethane (Baker, HPLC grade).

Self-assembly of mPEG-b-PMCL-PDMAEMA triblock copolymers

3D supramolecular assemblies of mPEG-b-PMCL-PDMAEMA triblock copolymers were prepared by the co-solvent method.[20] Block copolymer was dissolved in ethanol, and then a phosphate buffer saline solution (PBS) was added drop-wise to produce a copolymer concentration of 5 mg mL-1. The average size of the self-assembled nanoparticles was reduced by repeated extrusions (9 times) through filters (0.4 μm pore diameter) using a mini extruder from Avanti-Polar Lipidics Inc. Biomolecule-copolymer 3D assemblies were prepared in a similar manner. The block copolymer was dissolved in ethanol, and then a solution of the biomolecule (BSA or ASM) in PBS at physiological pH was added drop-wise to the copolymer solution to reach a copolymer concentration of 5 mg mL^{-1}, and a biomolecule concentration of

0.058 mg mL^{-1}. The final mixture was stirred overnight at room temperature and then dialyzed for 48 h in buffer, changing the buffer (pH = 7.2) 6 times in order to remove protein excess.

Light scattering

Dynamic light scattering (DLS) and static light scattering (SLS) were measured using an ALV laser goniometer with a linearly-polarized He-Ne laser operating at a wavelength of 632.8 nm (JDS Uniphase). Copolymer solutions were maintained at a constant temperature of 20 ± 0.1 °C. Measurements were carried out by varying the scattering angle (θ) from 30 to 150° in 10° steps. The viscosity of the solutions was assumed equal to that of pure water at 20 °C (η = 1.0 cP). The time correlation function *G(t)* was determined with an ALV/LSE-5004 correlator. Diffusion coefficients at zero deviation (D_0) were evaluated from *G(t)* using both nonlinear decay-time analysis and the Laplace inversion method (CONTIN).

Transmission Electron Microscopy (TEM)

TEM micrographs were obtained with a Phillips EM400 electron microscope operating at 100 kV. Nanoparticles were negatively stained by adding 5 µL of 2 % uranyl acetate solution and deposited on a carbon-coated copper grid. Excess uranyl acetate was removed under vacuum.

Cryogenic-TEM

Nanoparticle suspensions in buffer (10 mM PBS, pH 7.2, 50 mM NaCl) (1 mg mL^{-1}) were deposited on glow-discharged carbon grids (Quantifoil, Germany) and blotted before quick-freezing in liquid ethane using a Vitribot plunge-freezing device (FEI Co.). The grids were stored in liquid nitrogen before transferring them into a cryo-holder (Gatan). Imaging was performed on

a Philips CM200 FEG TEM at 200 kV accelerating voltage in low-dose mode with a defocus value of about −4 μm

Fluorescence Correlation Spectroscopy (FCS)

FCS was performed with a Zeiss LSM 510-META/Confcor2 laser-scanning microscope equipped with an Ar laser (488 nm) and a 40× water-immersion objective (Zeiss C/Apochromat 40X, NA 1.2), with the pinhole adjusted to 70 μm. Solutions of copolymers (5 mg/ml) with entrapped protein (BSA-FITC, $\lambda_{excitation}$ 495 nm) or enzyme (o-ASM, $\lambda_{excitation}$ 496 nm) were measured at room temperature in special chambered quartz-glass holders (Lab-Tek; 8-well, NUNC A/S), which provide optimal conditions for measurement while reducing evaporation of the solutions. Intensity fluctuations were analyzed using an autocorrelation function with the LSM 510/Confocor software package (Zeiss, AG). Spectra were recorded over 10 s, and each measurement was repeated ten times; results are reported as the average of three independent experiments. Adsorption and bleaching effects were reduced by exchanging the sample droplet after 2 minutes of measurement. The excitation power of the Ar laser was P_L = 200 mW, and the excitation transmission at 495 nm was 25 %. To reduce the number of fitting parameters, the diffusion times for free labeled protein (τ_D BSA-FITC = 82 μs) and for free labeled enzyme (τ_Do-ASM = 126μs) were independently determined, and fixed in the fitting procedure.

Cell toxicity assay

The [3-(4,5-dimethyl-2-yl)-5-(3-carboxymethoxyphenyl)-2-(4-sulfophenyl)-2H-tetrazolium (MTS) assay (Promega) was used to asses cell viability. Hela cells were cultured at a density of $2.5x10^3$ cells/well in a 96-well plate. After 24 hours, the medium was removed and 100 μl

aliquots containing the corresponding concentration of samples [0.5; 5 and 50 μg/ml] were added to the cell medium. Cells incubated only in medium served as controls. After 24 hours of incubation 20μl of MTS solution was added to each well. The plates were incubated for 2 hours at 37 ºC, and the absorption measured at λ = 490 nm. The quantity of formazan product as measured by absorbance at 490 nm is directly proportional to the number of living cells in culture. Absorption of cells where no nanoparticles were added served as 100 %.

Uptake of labeled-sphingomyelinase/PEG-b-PMCL-b-PDMAEMA

HeLa cells were cultured at a density of $5x10^4$ cells per well in an 8-well Lab-Tek (NalgeNunc International, USA) for 24 h in Dulbelcco's Modified Eagle's Medium (DMEM) containing 10% fetal calf serum (FCS) growth medium to allow attachment to the surface. After attachment, the medium was removed and nanoparticles containing fluorescent labeled Sphingomyelinase (o-ASM) (S.I) at a final polymer concentration of 0.05 mg/ml were incubated for an additional 24 h in DMEM growth medium. The pre-treated HeLa cells containing the o-ASM-nanoparticles were further incubated at 37 °C for 10 min with freshly prepared Deep Red (Cellmask) plasma membrane stain (5 mg/ml), and Hoechst 3342 (5 mg/ml) DNA stain. Cells washed three times with PBS were visualized with a CLSM (Carl Zeiss LSM510, Germany) equipped with a 63x water emulsion objective (Olympus, Japan). The measurements were performed in multitrack mode and the intensity of each fluorescent dye was adjusted individually: Hoechst 3342 was excited at 405 nm in channel 1, Deep Red at 633 nm in channel 2 and Alexa-488 at 488 nm in channel 3. The micrographs were recorded using Carl Zeiss LSM software (version 4.2 SP1).

Fluorescent-activated cell sorting (FACS)

$8x10^4$ HeLa cells were cultured in a well of a 24-well plate and cultured in DMEM containing 10% FCS for 24 h at 37 °C in a humidified CO_2 incubator. Then the medium was exchanged and polymer solution with entrapped biomolecule was added and incubated for another 24 h. Cells were washed with PBS, trypsinized, centrifuged, washed, centrifuged, suspended in PBS and put on ice. Flow cytometry was measured with a BD FACSCanto II flow cytometer (BD Bioscience, USA) using FSC and SSC detectors as well as a fluorescence channel o-ASM. A total of 20,000 events for each sample were analyzed, and data processed using Flowing Software 2.5.0 (Turku Centre for Biotechnology, Finland)

Enzyme activity assay

ASM release kinetics from PEG-*b*-PMCL-*b*-PDMAEMA nanoparticles incubated at physiological pH and acidic pH 5.5 (corresponding to lysosomal pH) were studied at room temperature. Nanoparticles containing no enzyme were measured to determine the background signal. The enzyme kinetics of ASM was followed immediately after mixing the sample with the Sphingomyelinase Assay Kit (Abcam®) in Microtiter® 96-Well FluorescenceMicroplates (Thermo Scientific). Enzyme was measured at pH 7.2 for the samples incubated at both pH 5.5 and 7.2 (SI).

Titration of PEG-b-PMCL-b-PDMAEMA nanoparticles

Nanoparticles for titration were prepared by the same method used for self-assembly at pH 7.2. A Zetasizer NANO with a multi-purpose titrator MPT-2 from Malvern was used, and NaOH (0.5 M), HCl (0.5 M) and HCl (0.05 M) solutions were used to adjust the pH between 3 and 10.

RESULTS AND DISCUSSION

PEG-*b*-PMCL-*b*-PDMAEMA tri-block copolymers were obtained by a three step synthesis: (*i*) ring-opening polymerization of γ-methyl-ε-caprolactone (MCL), (*ii*) functionalization of PEG-PMCL with an ATRP-initiating group, and (*iii*) ATRP of DMAEMA with mPEG-b-PMCL-Br as macronitiator. [20] Tri-block copolymers were assigned as $A_{45}B_mC_n$ where *m* and *n* represent the chain length of PMCL and PDMAEMA groups respectively determined from the ^{1}H NMR spectra (Figure S1, SI).

Self-assembly and characterization of PEG-b-PMCL-b-PDMAEMA copolymers

Self-assembly of PEG-*b*-PMCL-*b*-PDMAEMA (PEG_{45}-*b*-$PMCL_{110}$-*b*-$PDMAEMA_{37}$ and PEG_{45}-*b*-$PMCL_{101}$-*b*-$PDMAEMA_{27}$) copolymers was performed at various pH values in the range 3.5 - 10 in order to analyze both the 3D assemblies generated in dilute solutions, and their pH responsiveness. Supramolecular architectures of the copolymers were characterized by a combination of light scattering (dynamic and static), and TEM. TEM micrographs of self-assembled nanostructures of copolymers show the coexistence of two populations of spherical objects with different sizes (Figure 1 A, B).

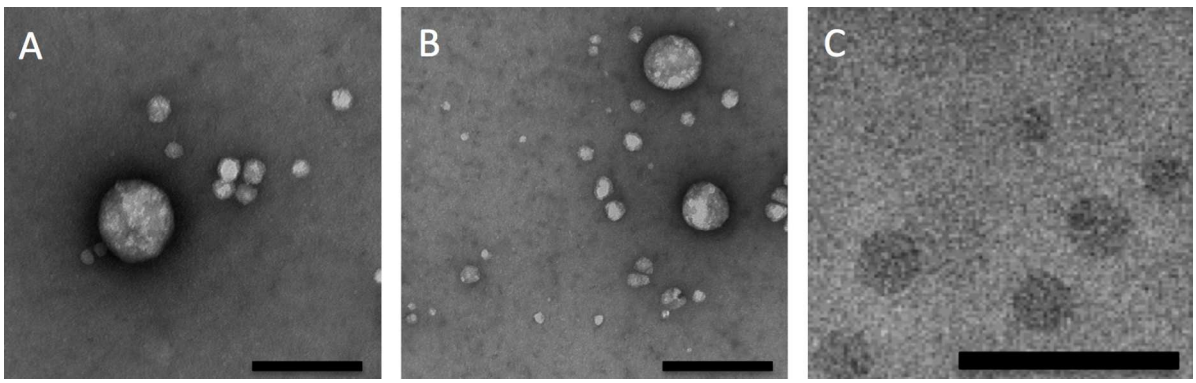

Figure 1. TEM micrographs of 3D supramolecular assemblies generated by PEG-*b*-PMCL-*b*-PDMAEMA copolymers at physiological pH. A. $A_{45}B_{110}C_{37}$ copolymer, B. $A_{45}B_{101}C_{27}$

copolymer. Scale bars: 200nm. C. Cryo-TEM micrograph of 3D supramolecular assemblies of $A_{45}B_{110}C_{37}$ copolymer after 2 months. Scale bar: 200 nm.

In this particular case, the size distribution of the spherical objects was measured by DLS to analyze the predominance of populations. According to the CONTIN algorithm, there are two populations of spherical objects: a population of particles with R_H~ 100 nm, and a second one with smaller particles of R_H~ 50 nm (Figure S2, SI). However, the existence of two separated populations allows us to analyze the data by taking into account only the population of particles with larger size. We calculated the ratio (ρ) between the radius of gyration (R_g), obtained from SLS, and the hydrodynamic radius (R_H), from DLS experiments ($\rho = R_g/R_H$), because it is known to be a specific parameter for identification of the morphology of spherical nano-objects (Table 1). ρ values of the 3D supramolecular assemblies of our copolymers were 1.19 - 1.23, which characterize an architecture of soft spherical nanoparticles with a hydrophilic corona, in agreement with previous reports [22]. A value for R_H larger than that obtained from TEM was expected, because the R_H from DLS experiments is the sum of the particle size and its surrounding hydration sphere.

Table 1. Physico-chemical parameters of PEG-*b*-PMCL-*b*-PDMAEMA copolymers in physiological conditions (PBS, pH 7.2 at 25 °C).

Copolymer	M_w (g/mol)[a]	ζ potential (mV)*	R_H (nm)	R_g (nm)	R_g/R_H	PDI
$A_{45}B_{110}C_{37}$	22100	20.2 ± 0.3	88 ± 10	112 ± 8	1.27	1.50

$A_{45}B_{101}C_{27}$	18167	12.9 ± 0.2	50 ± 12	66 ± 6	1.32	1.30

R_H: hydrodynamic radius; R_g: radius of gyration; *a. M_W, weight-average molar mass

At pH = 7.2, the radius of nanoparticles increased from 50 nm up to 88 nm, when the length of the B and C blocks increased (from 101 to 110 units for the B block and from 27 to 37 units for the C block). Under physiological pH, nanoparticles were stable for more than two months, as indicated by cryo-TEM and TEM micrographs (Fig. 1 C, S3, SI). In addition, cryo-TEM micrographs indicate a soft-core particle morphology for these assemblies, in the self-assembly conditions used here, specifically selected for attachment of proteins relevant for bio-applications.

Particle architecture and size are influenced by various factors such as: chemical nature of the blocks, chain length of each block and the ratio between them, the domain of the polymer exposed to the environment, pH and temperature. Therefore we analyzed the changes in the architecture and size of nanopoarticles at different pH values. By changing the pH, the particle size for each copolymer changed, indicating a pH sensitive behavior (Figure 2, Figure S3). The hydrodynamic radius, R_H, was affected both by the pH (3.5 – 12.0), and the molecular properties of the copolymers: D_H increased from 50±8 to 150±22 nm for $A_{45}B_{101}C_{27}$, and from 72±11 to 174±26 nm for $A_{45}B_{110}C_{37}$ nanoparticles. Whilst the size of $A_{45}B_{101}C_{27}$ nanoparticles did not change for pH values 6.0 - 7.4, $A_{45}B_{110}C_{37}$ nanoparticles increased their size in this pH range. The increase of the hydrodynamic radius upon increase of the pH is associated with the decrease of the electrostatic repulsions, which induces a starting of an aggregation process of the small nanoparticles.[23,24] The aggregation process can lead to a probable sedimentation of big aggregates as indicated by the SLS experiments (Figure S4). The equilibrium between the two

fractions of nanoparticles is shifted towards the smaller nanoparticles (SI, Figure S2 B).. With increasing pH, the particles lose their charge and the equilibrium shifts to larger nanoparticles, due to the start of a particle-particle aggregation process.

The pH sensitive behavior of PEG-*b*-PMCL-*b*-PDMAEMA soft nanoparticles indicates that the polymer domain exposed at the interface with the environment is predominantly PDMAEMA with possible PEG chains as well. Whilst there is no power to separate PEG and PDMAEMA, by taking into account the molecular characteristics of PEG and PDMAEMA monomers, PEG is not likely to be located at the external surface of the corona because of the bulky conformation of PDMAEMA for both copolymers. The resulting nanoparticle morphology is therefore based on PEG mainly embedded in the hydrophilic domain, and the branched PDMAEMA exposed at the particle surface. This privileged orientation of the PDMAEMA domain is exactly the one necessary to support attachment of biomolecules based on electrostatic interactions. In addition, note that only a small number of PEG chains can be located at the exterior domain with the environment to not obstruct protein attachment because of the repellent property of PEG. [25,26]

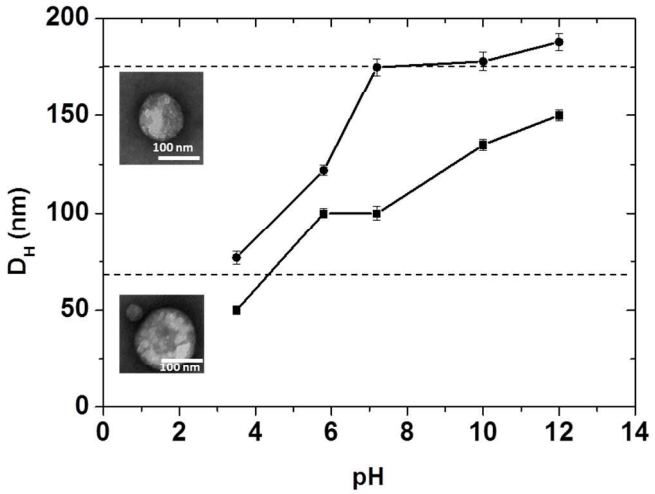

Figure 2. Hydrodynamic diameter (D_H) of PEG-*b*-PMCL-*b*-PDMAEMA NP. $A_{45}B_{110}C_{37}$ nanoparticles (circles), and $A_{45}B_{101}C_{27}$ nanoparticles (squares) at different pH values. Dashed lines represent a transition domain where both small and large nanoparticles co-exist.

The effect of temperature on the hydrodynamic diameter of nanoparticles was assessed between 25 and 40°C, a range relevant for medical applications. There was only a small change in nanoparticle diameter between 25 and 40ºC, which would not affect the possible medical application of the nanoparticles (Figure S5, SI).

Attachment of small molecular mass molecules to PEG-b-PMCL-b-PDMAEMA soft nanoparticles

Sodium fluorescein (Mw = 376.27 Da) was used as a model molecule to establish whether small molecular mass molecules can be attached to the nanoparticles. We used fluorescence correlation spectroscopy, FCS to examine the interaction of sodium fluorescein with the soft nanoparticles, by measuring the diffusion time of free sodium fluorescein, and sodium fluorescein-nanoparticles, respectively. In FCS, the laser-induced fluorescence of the excited fluorescent molecules that pass through a very small probe volume is auto-correlated in time to give information about the diffusion times of the molecules. These provide information about interactions of the fluorescent molecules with larger target molecules, including encapsulation/attachment of proteins in/to nanoparticles due to their proportionality to the R_H of the fluorescent object (according to the Stokes-Einstein equation). The change of the diffusion time for the free dye of τ_D =38 μs to 5.5 ms (for $A_{45}B_{101}C_{27}$ nanoparticles), and 5.9 ms (for $A_{45}B_{110}C_{37}$ nanoparticles) indicates that the dye interacts with both types of nanoparticle.

Electrostatic interactions represent the driving force for the attachment of sodium fluorescein, and attachment efficiencies (A.E) of 40% and 67%, respectively were obtained when the hydrophobic/hydrophilic ratio between the C and B blocks was increased (SI, Table S1). As expected, nanoparticles with a longer positively charged C block are able to attach more molecules (67%) than those with a shorter positively charged C block (40%).

Attachment of proteins to PEG-b-PMCL-b-PDMAEMA soft nanoparticles

A further step was to select model proteins and analyze whether they bind to PEG-b-PMCL-b-PDMAEMA soft nanoparticles. Water soluble bovine serum albumin (BSA) was selected because of its negatively charged backbone for pH > PI (isoelectric point PI = 4.7 at 25°), which favours its binding to the positively charged nanoparticles. The isoelectric point of the copolymers was determined by titration (Figure S6, SI), and attachment of BSA labelled with fluorescein isothiocyanate (FITC) to the nanoparticles was studied by FCS. The diffusion time (τ_d) for the free BSA-FITC at room temperature was τ_D = 82 μs (Figure S7 A-a and B-a, SI), and the autocorrelation curve for BSA-FITC-nanoparticles (Figure S7 A-b and B-b, SI) indicates the presence of slowly diffusing particles for both copolymers. This population with a reduced diffusion time, τ_D = 5.71 ms (for $A_{45}B_{110}C_{37}$), and τ_D = 5.53 ms (for $A_{45}B_{101}C_{27}$) represents more than 73 % of the total number of fluorescent particles that passed through the confocal volume during the measurement time, and corresponds to BSA-FITC-nanoparticles. The remaining diffusing fluorescent particles correspond to free BSA-FITC molecules, which were not attached to nanoparticles, and were detected due to their high quantum yield, and the high sensitivity of FCS. Upon interaction with BSA-FITC, the hydrodynamic radius of protein-nanoparticles changed compared to the values obtained from light scattering data (Table 2). However, it is

known that there are differences between the hydrodynamic radius determined by FCS and DLS[27], and therefore this difference is not considered as relevant. Light scattering of labelled protein-loaded nanoparticles was excluded because of the interference of the fluorophore with the laser used in light scattering experiments.

The attachment efficiency was calculated as the number of fluorescent labeled proteins per nanoparticle in comparison with the theoretical maximum number of fluorescent labeled proteins per nanoparticle (SI). The maximum number is calculated by dividing the volume of the vesicle with the volume of the fluorescent protein. Due to the preparation method of the particles (co-solvent method), the radius used for calculations for A.E were the R_H. The attachment efficiency of the nanoparticles indicates that the proteins are present in the outer corona of the nanoparticles because of the PDMAEMA domain predominantly exposed at their external surface. Nanoparticles morphology, which combines the molecular specificity of PEG and PDMAEMA with the results of the proteins attachment, is indeed based on PEG mainly forming the outer part of the nanoparticle core of PMCL, which is embedded into the domain of the branched PDMAEMA as the particle surface. The presence of the PDMAEMA domain at the interface of the nanoparticles with the environment favored both a controlled localization of charged biomolecules, and their pH-sensitive release.

Note that the protein-ABC fraction represents the overall bound protein-nanoparticle population in a two-populations FCS fit (free protein fraction and bound-protein fraction), without distinguishing between different numbers of nanoparticles or different number of proteins/nanoparticle in various samples. A.E. values are the key parameters to analyze the differences between the protein binding to different copolymers nanoparticles.

Table 2. Attachment efficiency of BSA-FITC to PEG-b-PMCL-b-PDMAEMA nanoparticles.

Copolymer	IEP	τ_D free protein (μs)	τ_D protein-ABC (μs)	D_H^* (nm)	D_H^{**} (nm)	free protein fraction (%)	protein-ABC fraction (%)	A. E (%)
$A_{45}B_{110}C_{37}$	9.16	82	5533	140	126	27	73	22
$A_{45}B_{101}C_{27}$	7.5	82	3189	113	119	4	96	13

IEP: Isoelectric point; D_H: hydrodynamic radius (*) by FCS (**) by DLS; A.E: attachment efficiency; τ_D: diffusion time

The A.E. of BSA-FITC increased from 13 to 22 % when the size of the hydrophilic block PDMAEMA increased (Table 2). This effect is attributed to electrostatic interactions between the positively charged hydrophilic block and the negatively charged protein at pH 7.2, in agreement with reports indicating that positively charged nanoparticles entrap proteins with isoelectric points lower than pH 5.5.[28] The release of BSA-FITC protein as a function of time was evaluated by FCS (Figure S8, SI). At pH = 5.8, PEG-b-PMCL-b-PDMAEMA nanoparticles released up to 70 % of BSA-FITC independent of the hydrophobic/hydrophilic ratio of the copolymers.

A step further towards the development of a product for therapeutic applications was to produce sphingomyelinase-bound nanoparticles, and the fraction of sphingomyelinase labeled with OregonGreen 488 succinimidyl ester (o-ASM) bound to polymer nanoparticles was evaluated in a similar manner to that described in the preceding paragraph. The autocorrelation curve for the free labeled enzyme resulted in a diffusion time of τ_D = 126 μs, whereas a significant increase was observed when the enzyme was added to nanoparticles: τ_D = 4.15 ms for $A_{45}B_{110}C_{37}$, and τ_D = 3.33 ms for $A_{45}B_{101}C_{27}$ nanoparticles, respectively (Figure 3 A and B). Similar to the BSA attachment, this significant increase in diffusion time is attributed to interaction of the enzyme with the nanoparticles. The hydrodynamic diameter of protein-nanoparticles increased compared to that of BSA-nanoparticles as a result of both the differences

in molecular masses of the biomolecules, and higher attachment efficiency for ASM (Table 2 and 3). The stronger interaction of the enzyme molecules with both types of nanoparticle is indicated by the fraction of enzyme-nanoparticles of > 89%.

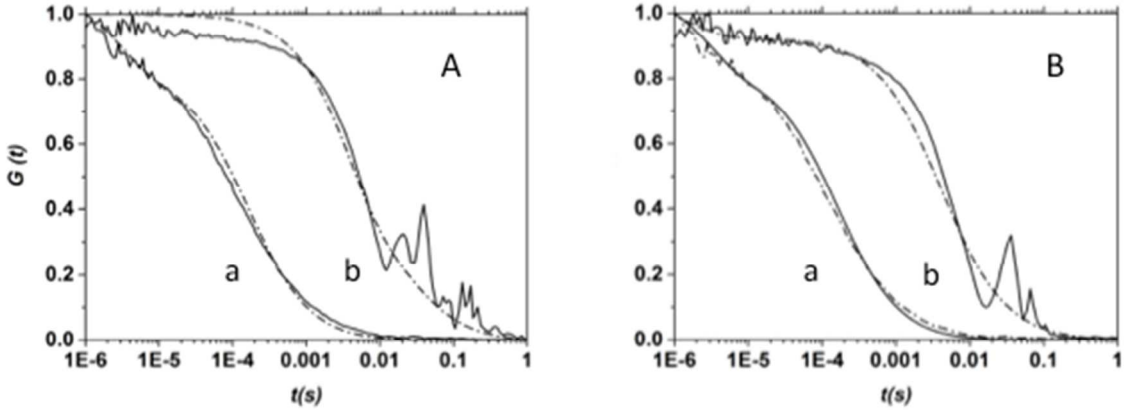

Figure 3. FCS autocorrelation curves (continuous lines) and their fits (dotted lines) for (A) free o-ASM (a) and o-ASM-nanoparticles of $A_{45}B_{110}C_{37}$ (b). (B) free o-ASM (a), and o-ASM-nanoparticles of$A_{45}B_{101}C_{27}$ (b). Curves are normalized to 1 to facilitate comparison.

Table 3.Attachment efficiency of o-ASM to PEG-b-PMCL-b-PDMAEMA (ABC) nanoparticles

Copolymer	τ_D free enzyme (μs)	τ_D enzyme-ABC (μs)	D_H (nm)	free protein fraction (%)	protein-ABC fraction (%)	N° molec/part	A.E (%)
$A_{45}B_{110}C_{37}$	126	4146	199	9	91	17	38
$A_{45}B_{101}C_{27}$	126	3326	143	11	89	11	13

The A.E. of molecules to polymer nanoparticles can be affected by several factors, such as method of preparation, size of the nanoparticles, hydrophilic/hydrophobic ratio, or concentration

of molecules to be attached.[29] In the case of PEG-b-PMCL-b-PDMAEMA nanoparticles, the particle size and the hydrophilic/hydrophobic ratio play an important role in the A.E., and results in an increase of > 50% when the sizes of the B and C blocks are increased. TEM micrographs (Figure S9, SI) show that attachment of proteins to PEG-b-PMCL-b-PDMAEMA nanoparticles does not affect the architecture of nanoparticles compared to those without attached proteins (Fig. 1).

Localization of proteins upon interaction with polymer nanoparticles is a key factor affecting the release profile. In the case of BSA-FITC attached to the outer interface of nanoparticles of PEO-PCL-PDMAEMA copolymers, protein localization at the external interface has been reported to improve the release behavior.[10] In order to get more insight into the localization of ASM upon interaction with the copolymer nanoparticles, we used a combination of zeta potential characterization and FCS. Zeta potential was measured for PEG-b-PMCL-b-PDMAEMA nanoparticles with and without enzyme (Figure S10, SI). Nanoparticles without ASM were positively charged (+15 mV), but on ASM addition, the charge of biomolecule-nanoparticles decreased dramatically (to -2 mV). This significant charge difference indicates that ASM molecules interact with the outer shell of the nanoparticles, in agreement with the morphology of the nanoparticles with the PDMAEMA domain exposed towards the environment. Localization of ASM molecules at the external hydrophobic domain of the soft nanoparticles was assessed by comparing the fraction of o-ASM-nanoparticles with the fraction of o-ASM molecules interacting with nanoparticles already attached to non-labeled ASM. First, copolymer nanoparticles ($A_{45}B_{101}C_{27}$ or $A_{45}B_{101}C_{37}$) without protein are prepared, then mixed with a solution of o-ASM during 50 minutes and measured by FCS. The autocorrelation function of free o-ASM and copolymer nanoparticle/o-ASM after mixing is shown in (Figure S11, SI). The

change in the autocorrelation function of the mixture of o-ASM with nanoparticle compared with that of the free o-ASM indicated that the proteins interacted with the outer corona of nanoparticles for both copolymers (Figure S11, SI), and an A.E of around 13 % was calculated for $A_{45}B_{101}C_{27}$. Second, nanoparticles were prepared in the presence of unlabeled ASM and measured by FCS both before and after addition of a solution of o-ASM for 50 minutes (Figure S11, SI). A significant decrease of the A.E to < 3% indicates that unlabeled-ASM molecules are already attached to the nanoparticles and hinder supplementary interaction of o-ASM with the nanoparticles. Therefore, ASM is mainly localized in the outer hydrophilic domain of nanoparticles, a location which favors protein release under appropriate environment conditions (Scheme 1).

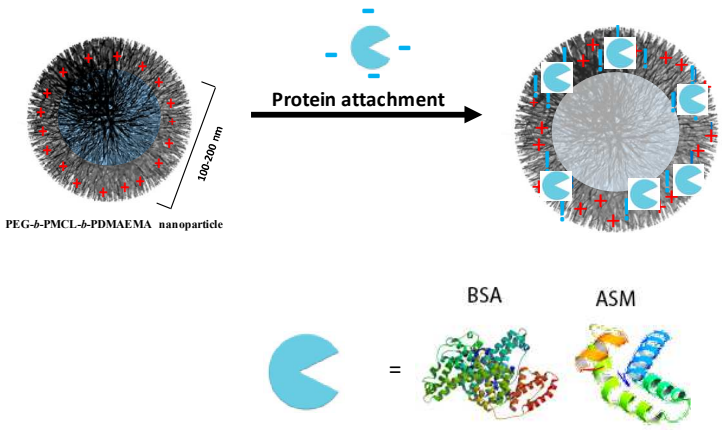

Scheme 1. Schematic illustration of the self-assembly of PEG-*b*-PMCL-*b*-PDMAEMA copolymers before and after interaction with a charged protein at pH 7.2.

A key parameter for potential medical applications is the activity of ASM upon interaction with the nanoparticles. Since ASM is stable in acidic conditions,[18] its activity was measured at pH 7.2 both for ASM-$A_{45}B_{110}C_{37}$ nanoparticles kept at this pH value, and for those previously

exposed to acidic conditions for 60 min (pH = 5.5) (Figure 4). The activity of ASM-$A_{45}B_{110}C_{37}$ kept at pH 7.2 was lower than that of ASM-particles previously exposed to acidic conditions due to the lower accessibility of ASM molecules at pH 7.2, being protected in the hydrophilic corona of the nanoparticles. The location of the proteins at the external hydrophilic domain of the nanoparticles is clearly supported by the residual enzymatic activity of the protein-loaded nanoparticles at pH 7.2. If the proteins would have been located in the inner domain of the nanoparticles, their accessibility would have been completely blocked and they should have no activity. The residual activity proves that the ASM proteins are located in the external hydrophilic domain being still able to convert the substrate into product. In the case of ASM-nanoparticles exposed at acidic pH, the more positively charged environment favors ASM release, which results in a significantly increase of the ASM activity.

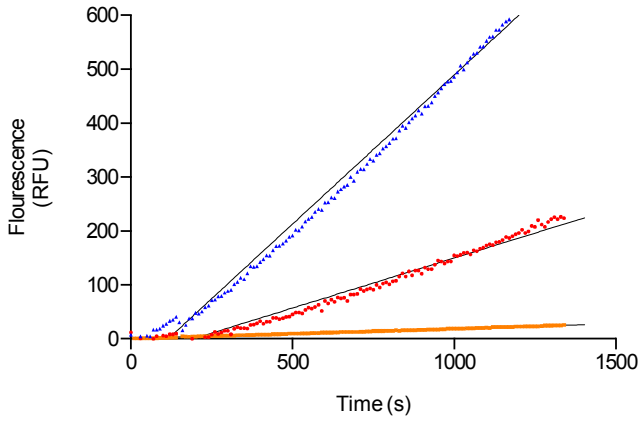

Figure 4: Enzymatic activity of ASM measured at pH 7.2: ASM-$A_{45}B_{110}C_{37}$ nanoparticles kept at pH 7.2 (Red), and ASM-$A_{45}B_{110}C_{37}$ nanoparticles exposed at pH 5.5 for 60 min (Blue); $A_{45}B_{110}C_{37}$ nanoparticles (Yellow).

Release of o-ASM was monitored by FCS for $A_{45}B_{110}C_{37}$ (Figure 5A) and $A_{45}B_{101}C_{27}$ (Figure 5B) as a function of time and pH. At pH 5.5, the release profile of ASM- $A_{45}B_{110}C_{37}$ nanoparticles shows a fast ASM release within 240 min (70 %), followed by a plateau (around 85 % release). The fast release profile is due to favored diffusion of ASM from the corona of the nanoparticles, because of the combined effect of the decreased charge of the protein molecules (pH < I.P) and the increased positive change of the environment. The fast release can be correlated with the increased activity of ASM-nanoparticles in acidic pH conditions (see above). At pH 7.2, as the proteins are negatively charged, electrostatic interactions favor their attachment to the nanoparticles, which results in a significantly slower release (30 % release in 240 min). A similar release of ASM molecules was observed at pH = 7.2 for nanoparticles based on copolymers with a shorter C block. However, a slower release profile was observed at pH = 5.5 in the case of $A_{45}B_{101}C_{27}$ nanoparticles compared to that resulting from $A_{45}B_{110}C_{37}$ nanoparticles: the decreased fraction of the released protein molecules from nanoparticles based on a shorter C block is due to a different balance in the electrostatic interactions, because of the different amount of attached proteins (Table 3).

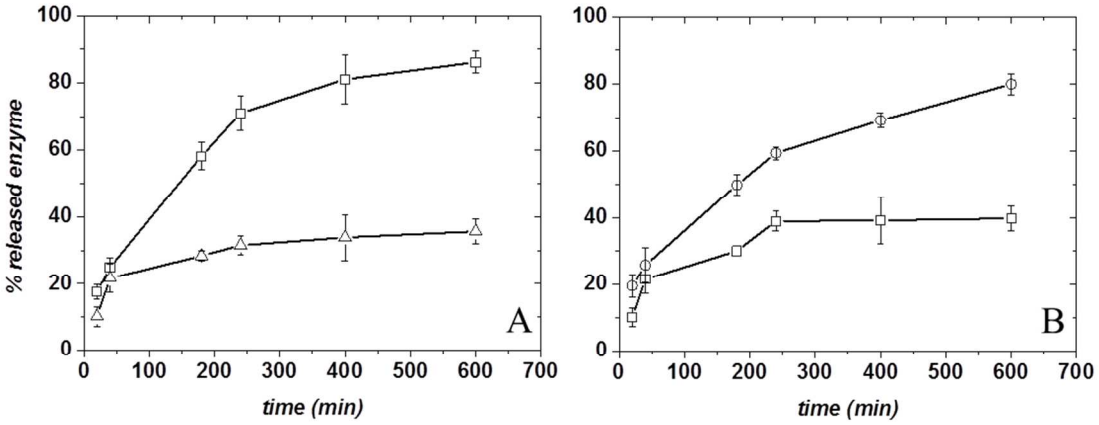

Figure 5. Release behavior of o-ASM from ABC nanoparticles as a function of time: (A) $A_{45}B_{110}C_{37}$ nanoparticles at pH 7.2 (triangles), and at pH 5.5 (squares). (B) $A_{45}B_{101}C_{27}$ nanoparticles at pH 7.2 (squares) and at pH 5.5 (circles).

Cell toxicity and uptake of PEG-b-PMCL-b-PDMAEMA nanoparticles

The toxicity of nanoparticles was assessed in HeLa cell lines using the MTS assay (SI) by incubating for 24 hours with nanoparticles, BSA- or ASM-nanoparticles (concentrations up to 50 μg/ml). The nanoparticles and both protein-loaded nanoparticles all showed >70% cell viability (Figure 6).

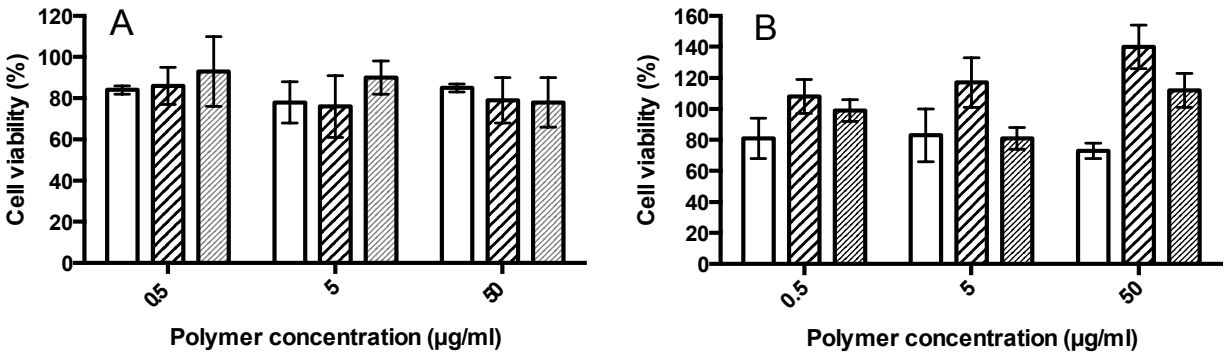

Figure 6. HeLa cell viability after 24 h incubation with nanoparticles. (A) $A_{45}B_{110}C_{37}$ nanoparticles (empty), $A_{45}B_{110}C_{37}$ nanoparticles with BSA-FITC (stripes), $A_{45}B_{110}C_{37}$ nanoparticles with o-ASM (dense stripes). (B) $A_{45}B_{101}C_{27}$ nanoparticles (empty), $A_{45}B_{101}C_{27}$ nanoparticles with BSA-FITC (stripes), and $A_{45}B_{101}C_{27}$ nanoparticles with o-ASM (dense stripes).

At the highest concentration $A_{45}B_{101}C_{27}$ nanoparticles present a slightly lower cell viability (73%) than $A_{45}B_{110}C_{37}$ nanoparticles (78%), due to a lower overall positive charge (ESI), in agreement with previous reports on cationic polymer nanoparticles. [30] However, upon attachment of protein molecules, both $A_{45}B_{101}C_{27}$ and $A_{45}B_{110}C_{37}$ nanoparticles at the highest concentration have a lower cytotoxicity (the effect is, due to the decrease in the overall positive charge, as indicated by zeta-potential measurements (Fig. S8, SI). The effect is seen for both copolymers, but it is more pronounced for $A_{45}B_{110}C_{37}$-based nanoparticles. BSA-FITC loaded $A_{45}B_{110}C_{37}$ nanoparticles presented a viability > 100%, due to the stimulatory effect of BSA on cell proliferation.[31] Overall, the low cytotoxicity of protein-nanoparticles supports their further development for therapeutic applications.

To be applied as a therapeutic agent, cellular uptake of ASM-nanoparticles is critical and therefore was investigated in HeLa cells using confocal laser scanning microscopy (CLSM). In HeLa cells incubated with the o-ASM/ABC nanoparticles for 24 h, the presence of a fluorescent signal for o-ASM/$A_{45}B_{110}C_{37}$ nanoparticles, and o-ASM/$A_{45}B_{101}C_{27}$ nanoparticles clearly indicated uptake of o-ASM loaded nanoparticles (Figure 7).

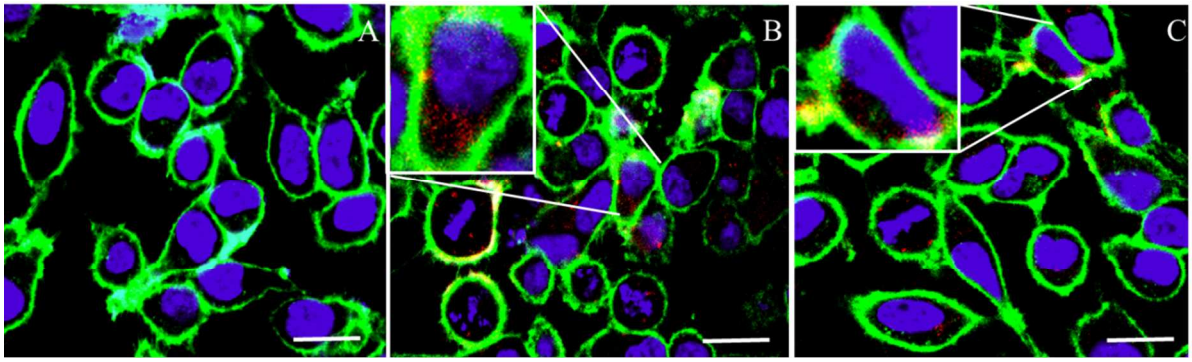

Figure 7. Confocal laser scanning micrographs of HeLa cells. The cellular membrane was visualized by Cell Mask Deep Red (green), nuclei with Hoechst 33342 (violet), and o-ASM

(red). A) Untreated cells, B) Cells treated with 50µg/ml o-ASM-$A_{45}B_{110}C_{37}$ nanoparticles, C) cells treated with 50µg/ml o-ASM-$A_{45}B_{101}C_{27}$ nanoparticles. Insets: zoomed regions of HeLa cells treated with 50µg/ml o-ASM-$A_{45}B_{110}C_{37}$ and 50µg/ml o-ASM-$A_{45}B_{101}C_{27}$ nanoparticles. Scale bar: 50 µm

In addition, up-take by HeLa cells after incubation for 24h of nanoparticles containing fluorescently labeled BSA-FITC (1:12 labeling efficiency) and o-ASM (1:3 labeling efficiency) respectively, was measured by fluorescence-activated cell sorting (FACS). A significant shift of the peaks corresponding to the cells incubated with nanoparticles compared to normal cells confirms uptake (Figure 8). The difference in fluorescence shift between nanoparticles loaded with BSA-FITC and o-ASM is attributed to the lower labeling efficiency of o-ASM. The stimulating effect of BSA is considered only as a minor factor, because the coating of nanoparticles with BSA has been reported to have little or no influence on the cellular uptake of nanoparticles[32].

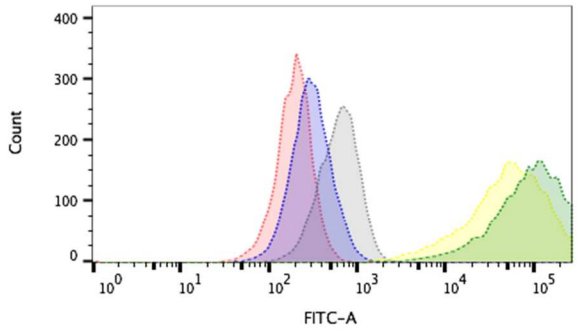

Figure 8. Flow cytometry analysis of cellular uptake of HeLa cells for labeled proteins in nanoparticles: Untreated HeLa cells (red); HeLa cells treated with 50µg/ml o-ASM-$A_{45}B_{101}C_{27}$ (blue); HeLa cells treated with 50µg/ml o-ASM-$A_{45}B_{110}C_{37}$ (grey); HeLa cells treated with

50μg/ml BSA-FITC-$A_{45}B_{101}C_{27}$ (yellow), and HeLa cells treated with 50μg/ml BSA-FITC-$A_{45}B_{110}C_{37}$ (green).

4. CONCLUSION

By self-assembly of as-symmetric poly(ethylenegycol)-b-poly(methyl caprolactone)-b-poly(2-(N,N-diethylamino) ethyl methacrylate) copolymers with two different ratios of the hydrophobic to hydrophilic blocks we generated soft nanoparticles to which proteins could be attached at a desired location in order to develop an efficient protein delivery platform. The asymmetry of the block copolymers favored a specific location for proteins and small molecular mass molecules: the PDMAEMA block predominantly present at the external interface favored attachment of proteins and small molecular mass molecules with the opposite charge, whilst PEG was mainly embedded inside the hydrophilic domain. Combination of the methods we used in this study (LS, TEM, cryo-TEM, FCS, activity assays of the proteins) allowed understanding the nanoparticles morphology and behavior in the presence of proteins as key factors for future translational applications. Attachment of biomolecules was favored by a triggered effect of electrostatic interactions between the PDMAEMA domain and negatively charged molecules. Both BSA and o-ASM were successfully attached, and subsequently released from the self-assembled nanoparticles (>80%) when the pH was decreased to acidic values. This is the first system based on electrostatic attachment and release of therapeutic proteins (ASM), whilst preserving their activity. The protein-polymer nanoparticles showed low toxicity at concentrations up to 50μg/ml, and were up-taken by HeLa cells. PEG-*b*-PMCL-*b*-PDMAEMA nanoparticles can attach a variety of biomolecules with charge opposite to that of the PDMAEMA domain, and then release them in a pH-responsive manner, which supports their further optimization for potential therapeutic applications. Our study is the first one showing that it is possible to deliver proteins

in a pH responsive manner by their controlled localisation in the nanoparticle interface with the environment.

ASSOCIATED CONTENT

Supporting Information.

This material is available free of charge via the Internet at http://pubs.acs.org.

AUTHOR INFORMATION

***Corresponding Author**

Prof. Dr. Cornelia G. Palivan

Cornelia.palivan@unibas.ch

Author Contributions

⊥These authors have contributed equally and should be co-first authors. All authors have given approval to the final version of the manuscript.

ACKNOWLEDGMENT

We gratefully acknowledge the financial support provided by the University of Basel, the Swiss Nanoscience Institute, and the Swiss National Science Foundation. D.V thanks G. Persy (University of Basel) for TEM-measurements. T.E thanks C. Labão (University of Basel) for fruitful discussions. Dr. M. Chami (University of Basel) is acknowledged for the cryo-TEM experiments, and Dr. B.A. Goodman for editing the manuscript.

REFERENCES

(1) Smales, C. M.; James, D. C. *Therapeutic Proteins*; Humana Press: New Jersey, **2005**; Vol. 308, 1-16

(2) Pisal, D. S.; Kosloski, M. P.; Balu-Iyer, S. V. Delivery of Therapeutic Proteins. *J. Pharm. Sci.* **2010**, *99*, 2557–2575.

(3) Najer, A.; Wu, D.; Vasquez, D.; Palivan, C. G.; Meier, W. Polymer Nanocompartments in Broad-Spectrum Medical Applications. *Nanomedicine* **2013**, *8*, 425–447.

(4) Govender, T.; Stolnik, S.; Garnett, M. C.; Illum, L.; Davis, S. S. PLGA Nanoparticles Prepared by Nanoprecipitation: Drug Loading and Release Studies of a Water Soluble Drug. *J. Cont. Release* **1999**, *57*, 171–185.

(5) Jahanshahi, M.; Babaei, Z. Protein Nanoparticle: a Unique System as Drug Delivery Vehicles *Afr. J. Biotechnol.* **2008**, *7* , 4926–4934.

(6) Saptarshi, S. R.; Duschl, A.; Lopata, A. L. Interaction of Nanoparticles with Proteins: Relation to Bio-Reactivity of the Nanoparticle. *J. Nanotechnol* **2013**, *11*, 1–1.

(7) Zhang, Y.; Zhuo, R.-X. Synthesis and in Vitro Drug Release Behavior of Amphiphilic Triblock Copolymer Nanoparticles Based on Poly (Ethylene Glycol) and Polycaprolactone. *Biomaterials* **2005**, *26*, 6736–6742.

(8) Guo, S.; Huang, Y.; Wei, T.; Zhang, W.; Wang, W.; Lin, D.; Zhang, X.; Kumar, A.; Du, Q.; Xing, J. Amphiphilic and Biodegradable Methoxy Polyethylene Glycol-Block-(Polycaprolactone-Graft-Poly(2-(Dimethylamino)Ethyl Methacrylate)) as an Effective Gene Carrier. *Biomaterials* **2011**, *32* , 879–889.

(9) Wittemann, A.; Ballauff, M. Interaction of Proteins with Linear Polyelectrolytes and Spherical Polyelectrolyte Brushes in Aqueous Solution. *Phys Chem Chem Phys* **2006**, *8*, 5269–5275.

(10) Wittemann, A.; Azzam, T.; Eisenberg, A. Biocompatible Polymer Vesicles From Biamphiphilic Triblock Copolymers and Their Interaction with Bovine Serum Albumin. *Langmuir* **2007**, *23* (4), 2224–2230.

(11) Lu, Y.; Sun, W.; Gu, Z. Stimuli-Responsive Nanomaterials for Therapeutic Protein Delivery. *J Control Release* **2014**, *194*, 1–19.

(12) Chu, X.-P.; Papasian, C. J.; Wang, J. Q.; Xiong, Z.-G. Modulation of Acid-Sensing Ion Channels: Molecular Mechanisms and Therapeutic Potential. *Int J Physiol Pathophysiol Pharmacol* **2011**, *3*, 288–309.

(13) Lee, Y.; Ishii, T.; Cabral, H.; Kim, H. J.; Seo, J.-H.; Nishiyama, N.; Oshima, H.; Osada, K.; Kataoka, K. Charge-Conversional Polyionic Complex Micelles-Efficient Nanocarriers for Protein Delivery Into Cytoplasm. *Angew. Chem. Int. Ed. Engl.* **2009**, *48*, 5309–5312.

(14) Yan, M.; Du, J.; Gu, Z.; Liang, M.; Hu, Y.; Zhang, W.; Priceman, S.; Wu, L.; Zhou, Z. H.; Liu, Z.; et al. A Novel Intracellular Protein Delivery Platform Based on Single-Protein Nanocapsules. *Nature Nanotechnology* **2010**, *5*, 48–53.

(15) Wu, X.; Wu, S.; Yang, L.; Han, J.; Han, S. Cytosolic Delivery of Proteins Mediated by Aldehyde-Displaying Silica Nanoparticles with pH-Responsive Characteristics. *J. Mater. Chem.* **2012**, *22*, 17121–17127.

(16) Cheng, C.; Convertine, A. J.; Stayton, P. S.; Bryers, J. D. Multifunctional Triblock Copolymers for Intracellular Messenger RNA Delivery. *Biomaterials* **2012**, *33*, 6868–6876.

(17) Guo, S.; Huang, Y.; Zhang, W.; Wang, W.; Wei, T.; Lin, D.; Xing, J.; Deng, L.; Du, Q.; Liang, Z.; et al. Ternary Complexes of Amphiphilic Polycaprolactone-Graft-Poly (N,N-

Dimethylaminoethyl Methacrylate), DNA and Polyglutamic Acid-Graft-Poly(Ethylene Glycol) for Gene Delivery. *Biomaterials* **2011**, *32*, 4283–4292.

(18) Edward H. Schuchman. Acid Sphingomyelinase, Cell Membranes and Human Disease: Lessons From Niemann–Pick Disease. *FEBS Lett.* **2010**, *584*, 1895–1900.

(19) Garnacho, C.; Dhami, R.; Simone, E.; Dziubla, T.; Leferovich, J.; Schuchman, E. H.; E. H.; Muzykantov, V.; Muro, Delivery of Acid Sphingomyelinase in Normal and Niemann-Pick Disease Mice Using Intercellular Adhesion Molecule-1-Targeted Polymer Nanocarriers. S. *J. Pharm. Exp. Ther.* **2008**, 325, 400–408.

(20) Matter, Y.; Enea, R.; Casse, O.; Lee, C. C.; Baryza, J.; Meier, W. Amphiphilic PEG-B-PMCL-B-PDMAEMA Triblock Copolymers: From Synthesis to Physico-Chemistry of Self-Assembled Structures. *Macromol. Chem. Phys.* **2011**, *212*, 937–949.

(21) Zupancich, J. A.; Bates, F. S.; Hillmyer, M. A. Aqueous Dispersions of Poly(Ethylene Oxide)- B-Poly(Γ-Methyl-E-Caprolactone) Block Copolymers. *Macromolecules* **2006**, *39*, 4286–4288.

(22) Karin Schillén; Ahmad Yekta; Shaoru Ni; J P S Farinha, A.; Winnik, M. A. Characterization of Polyisoprene-B-Poly(Methyl Methacrylate) Diblock Copolymer Micelles in Acetonitrile. *J. Phys. Chem. B*, **1999**, 103, 9099

(23) Car, A.; Baumann, P.; Duskey, J. T.; Chami, M.; Bruns, N.; Meier, W. pH-Responsive PDMS-B-PDMAEMA Micelles for Intracellular Anticancer Drug Delivery. *Biomacromolecules* **2014**, *15*, 3235–3245.

(24) Tebaldi, M. L.; Leal, D. A.; Montoro, S. R.; Petzhold, C. Synthesis of Stimuli-Sensitive Copolymers by RAFT Polymerization: Potential Candidates as Drug Delivery Systems. *Mat. Res.* **2014**, *17*, 191–196.

(25) Allen, C.; Santos, Dos, N.; Gallagher, R.; Chiu, G. N. C.; Shu, Y.; Li, W. M.; Johnstone, S. A.; Janoff, A. S.; Mayer, L. D.; Webb, M. S.; et al. Controlling the Physical Behavior and Biological Performance of Liposome Formulations Through Use of Surface Grafted Poly(Ethylene Glycol). *Biosci Rep* **2002**, *22*, 225–250.

(26) Elbert, D. L.; Hubbell, J. A. Surface Treatments of Polymers for Biocompatibility. *Annual Review of Materials Science* **1996**, *26*, 365–394.

(27) Wu, B.; Chen, Y.; Müller, J. D. Fluorescence Correlation Spectroscopy of Finite-Sized Particles. *Biophysical Journal* **2008**, *94*, 2800–2808.

(28) Rahman, M.; Laurent, S.; Tawil, N.; Yahia, L.; Mahmoudi, M. Nanoparticle and Protein Corona. In *Protein-Nanoparticle Interactions*; Springer Series in Biophysics; Springer Berlin Heidelberg: Berlin, Heidelberg, 2013; Vol. 15, pp 21–44.

(29) Hu, Y.; Xie, J.; Tong, Y. W.; Wang, C.-H. Effect of PEG Conformation and Particle Size on the Cellular Uptake Efficiency of Nanoparticles with the HepG2 Cells. *Journal of Controlled Release* **2007**, *118*, 7–17.

(30) vandeWetering, P.; Cherng, J. Y.; Talsma, H.; Hennink, W. E. Relation Between Transfection Efficiency and Cytotoxicity of Poly(2-(Dimethylamino)Ethyl Methacrylate)/Plasmid Complexes. *Journal of Controlled Release* **1997**, *49* (1), 59–69.

(31) Bedotti, R.; Borghetti, A. F.; Favilla, R. Stimulatory Effect of Serum Albumin on the Proliferation of Serum-Free SV40-Transformed Balb/C 3T3 Cells. *Biochim. Biophys. Acta* **1990**, *1053*, 74–80.

(32) Baier, G.; Costa, C.; Zeller, A.; Baumann, D.; Sayer, C.; Araujo, P. H. H.; Mailänder, V.; Musyanovych, A.; Landfester, K. BSA Adsorption on Differently Charged Polystyrene Nanoparticles Using Isothermal Titration Calorimetry and the Influence on Cellular

Uptake. *Macromol Biosci* **2011**, *11*, 628–638.

TOC Graphic

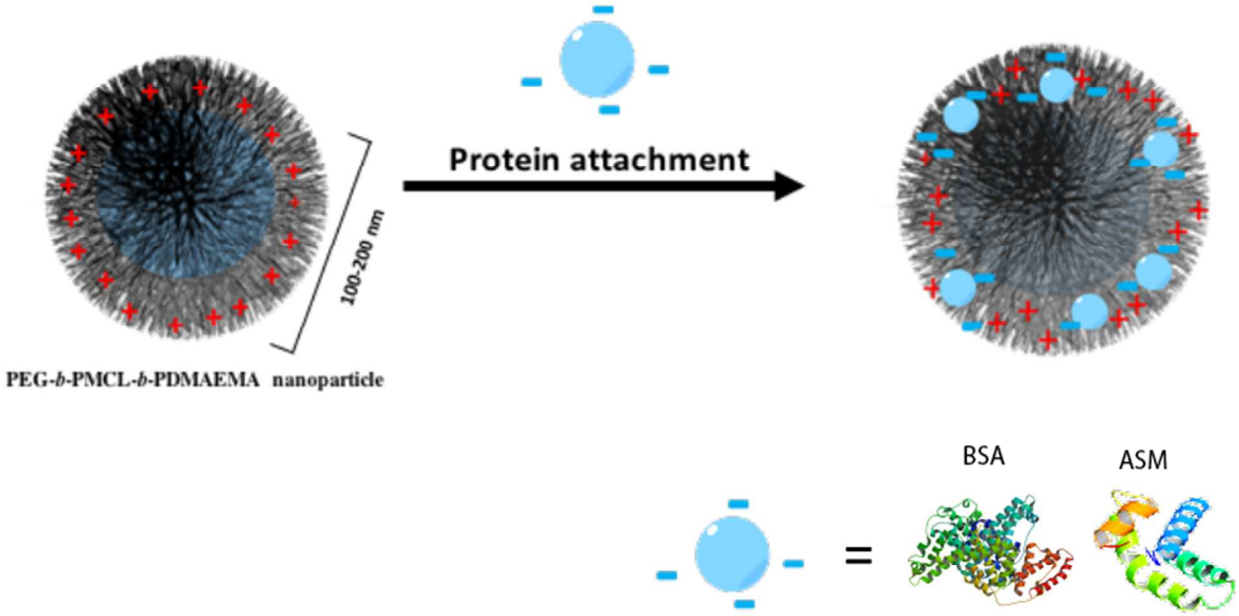
Protein attachment
100-200 nm
PEG-b-PMCL-b-PDMAEMA nanoparticle
BSA
ASM
=

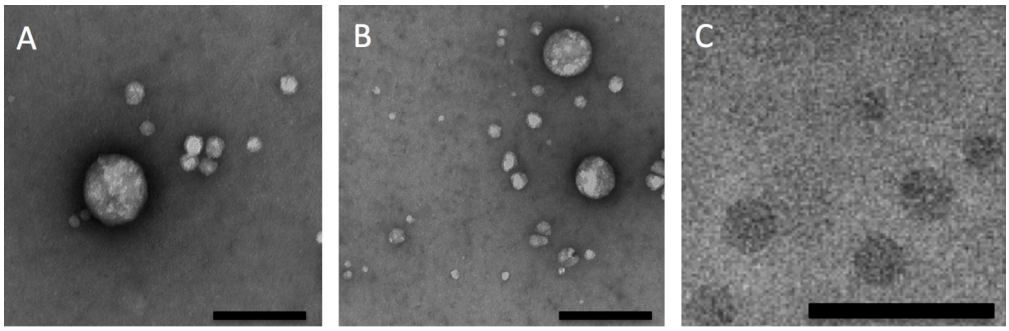

TEM micrographs of 3D supramolecular assemblies generated by PEG-b-PMCL-b-PDMAEMA copolymers at physiological pH. A. A45B110C37 copolymer, B. A45B101C27 copolymer. Scale bars: 200nm. C. Cryo-TEM micrograph of 3D supramolecular assemblies of A45B110C37 copolymer after 2 months. Scale bar: 200 nm.

598x191mm (72 x 72 DPI)

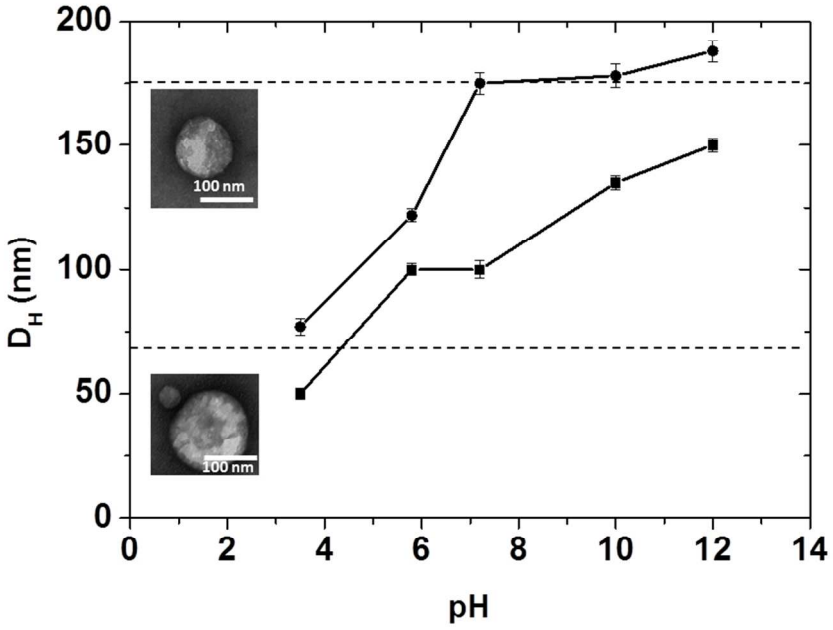

Hydrodynamic diameter (DH) of PEG-b-PMCL-b-PDMAEMA NP. A45B110C37 nanoparticles (circles), and A45B101C27 nanoparticles (squares) at different pH values. Dashed lines represent a transition domain where both small and large nanoparticles co-exist.

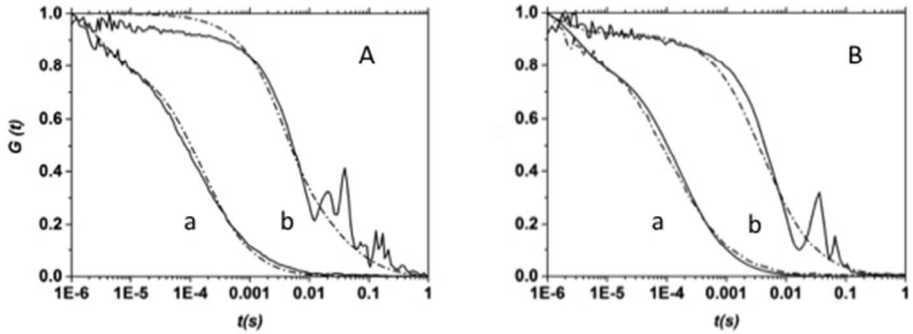

Figure 3. FCS autocorrelation curves (continuous lines) and their fits (dotted lines) for (A) free o-ASM (a) and o-ASM-nanoparticles of A45B110C37 (b). (B) free o-ASM (a), and o-ASM-nanoparticles ofA45B101C27 (b). Curves are normalized to 1 to facilitate comparison.

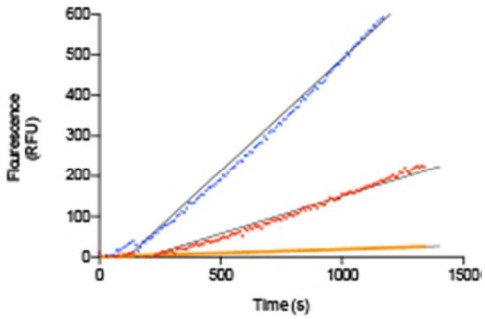

Enzymatic activity of ASM measured at pH 7.2: ASM-A45B110C37 nanoparticles kept at pH 7.2 (Red), and ASM-A45B110C37 nanoparticles exposed at pH 5.5 for 60 min (Blue); A45B110C37 nanoparticles (Yellow).

85x61mm (72 x 72 DPI)

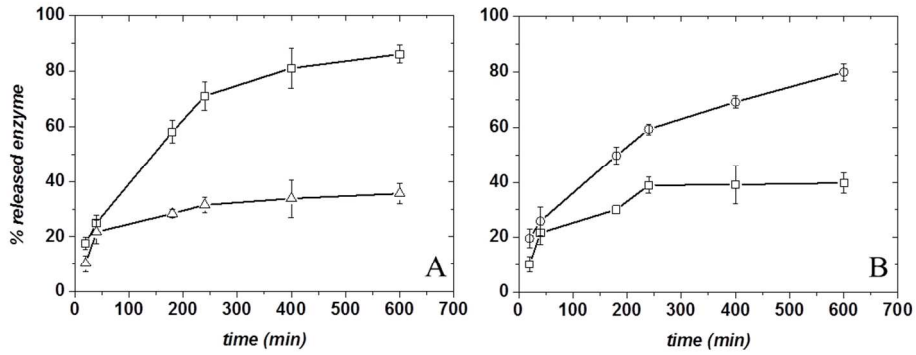

Figure 5. Release behavior of o-ASM from ABC nanoparticles as a function of time: (A) A45B110C37 nanoparticles at pH 7.2 (triangles), and at pH 5.5 (squares). (B) A45B101C27 nanoparticles at pH 7.2 (squares) and at pH 5.5 (circles).

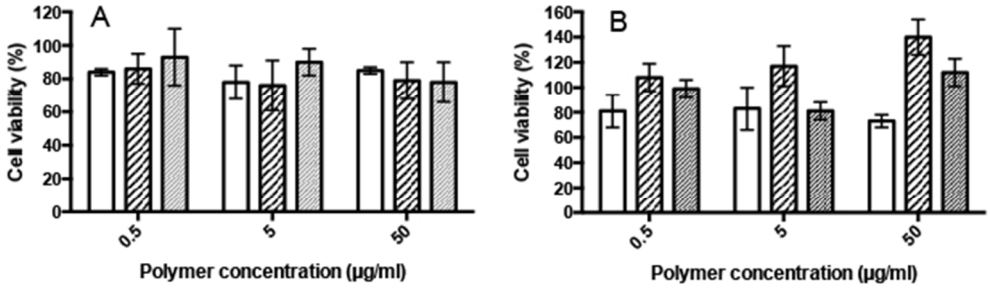

HeLa cell viability after 24 h incubation with nanoparticles. (A) A45B110C37 nanoparticles (empty), A45B110C37 nanoparticles with BSA-FITC (stripes), A45B110C37 nanoparticles with o-ASM (dense stripes). (B) A45B101C27 nanoparticles (empty), A45B101C27 nanoparticles with BSA-FITC (stripes), and A45B101C27 nanoparticles with o-ASM (dense stripes).

219x68mm (72 x 72 DPI)

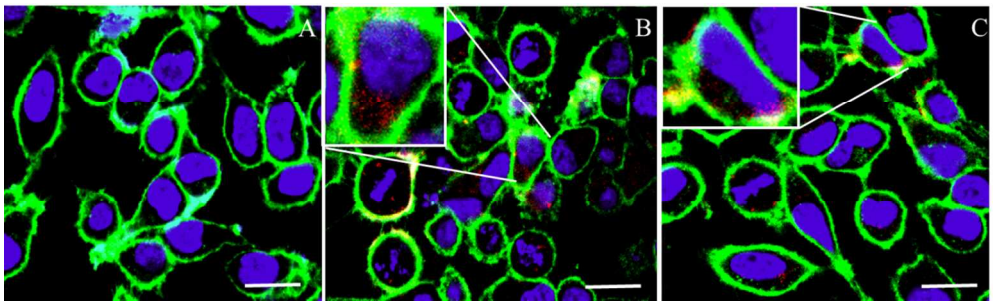

Confocal laser scanning micrographs of HeLa cells. The cellular membrane was visualized by Cell Mask Deep Red (green), ,nuclei with Hoechst 33342 (violet), and the fluorescent labeled ASM (red). A) Untreated cells, B) Cells treated with 50µg/ml o-ASM-A45B110C37 nanoparticles, C) cells treated with 50µg/ml o-ASM-A45B101C27 nanoparticles. Insets: zoomed regions of HeLa cells treated with 50µg/ml o-ASM-A45B110C37 and 50µg/ml o-ASM-A45B101C27 nanoparticles. Scale bar: 50 µm

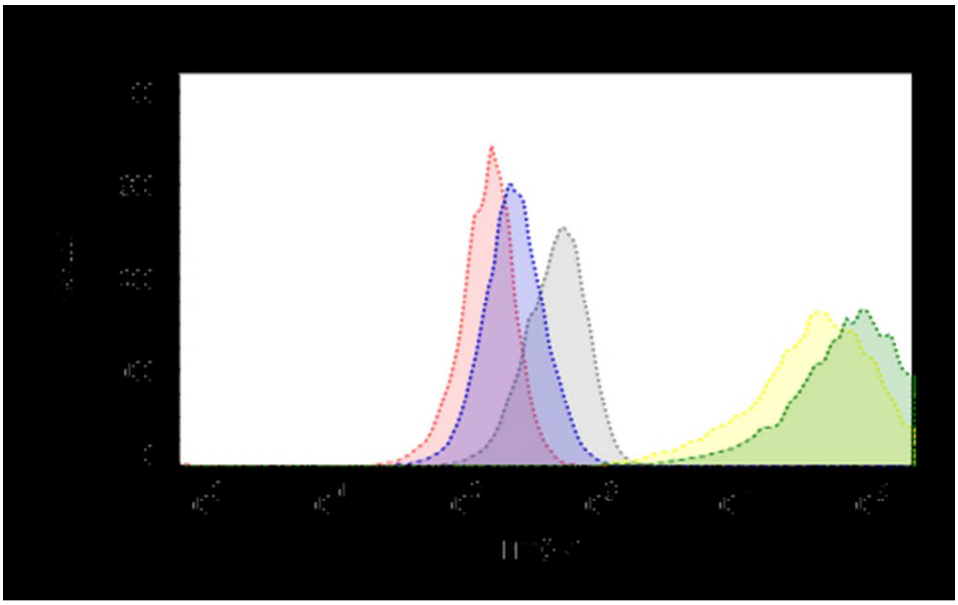

. Flow cytometry analysis of cellular uptake of HeLa cells for labeled proteins in nanoparticles: Untreated HeLa cells (red); HeLa cells treated with 50μg/ml o-ASM-A45B101C27 (blue); HeLa cells treated with 50μg/ml o-ASM-A45B110C37 (grey); HeLa cells treated with 50μg/ml BSA-FITC-A45B101C27 (yellow), and HeLa cells treated with 50μg/ml BSA-FITC-A45B110C37 (green).

12065x7543mm (1 x 1 DPI)

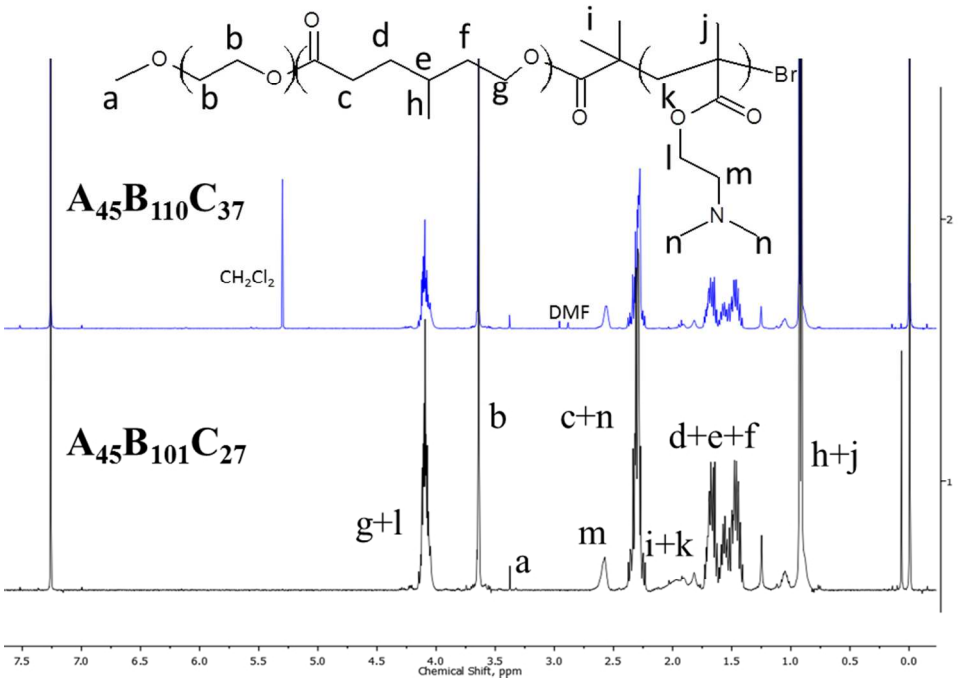

1H NMR spectra of ABC tri-block copolymers.

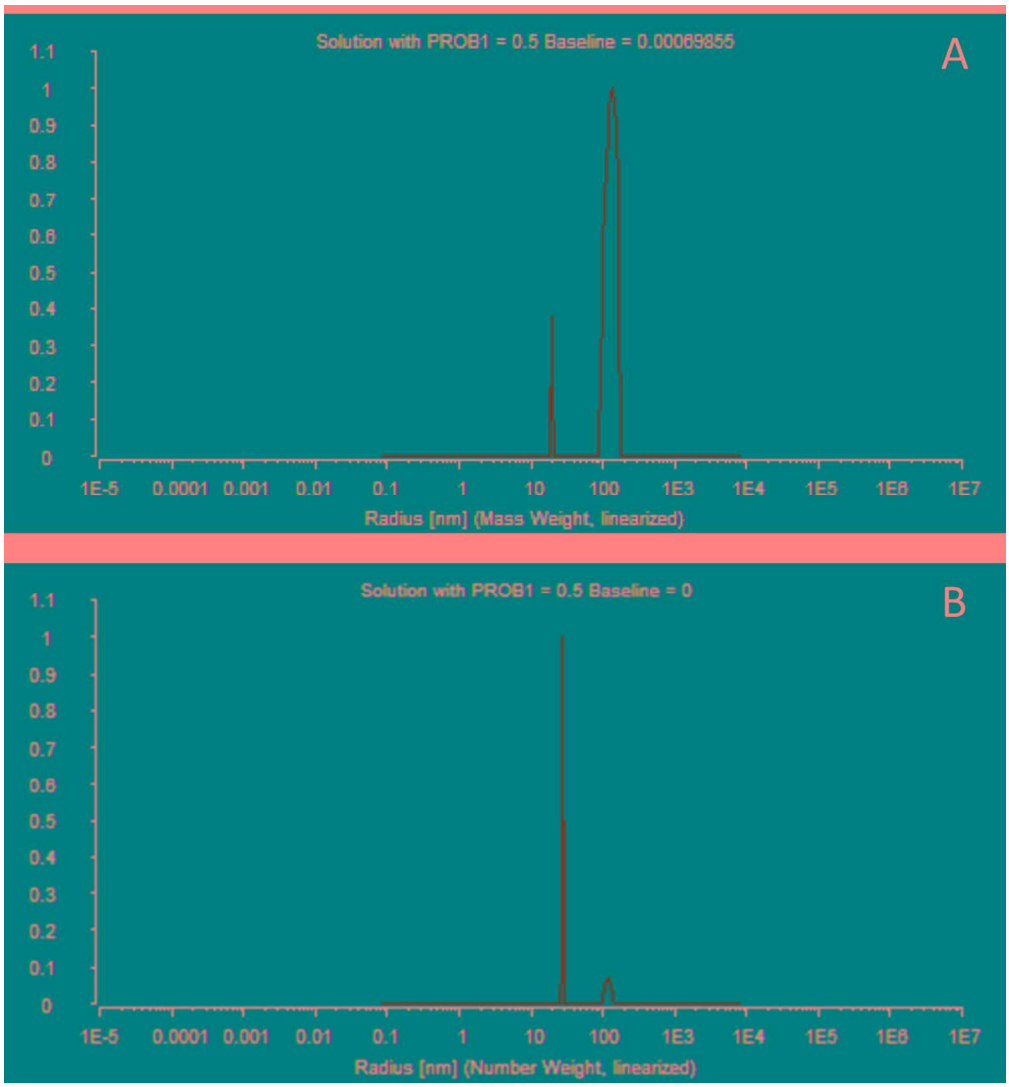

Particle size distribution of A45B110C37 tri-block copolymers. A.) Mass weighted distribution. B.) Number weighted distribution.

131x141mm (300 x 300 DPI)

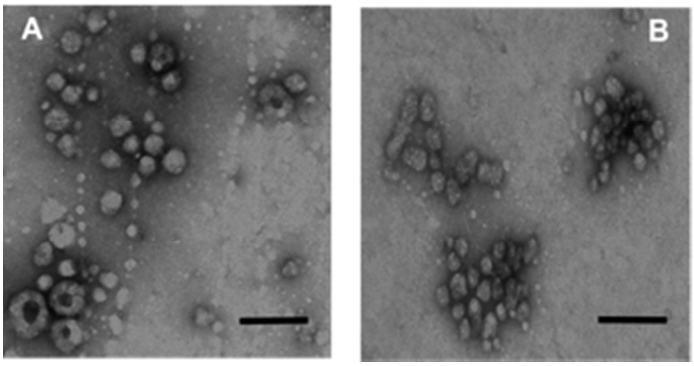

Figure S3: Transmision Electron Microscopy of A45B110C37 copolymer: (A) sample prepared at first day (B) sample after 60 days. Scale bar: 500 nm

121x63mm (72 x 72 DPI)

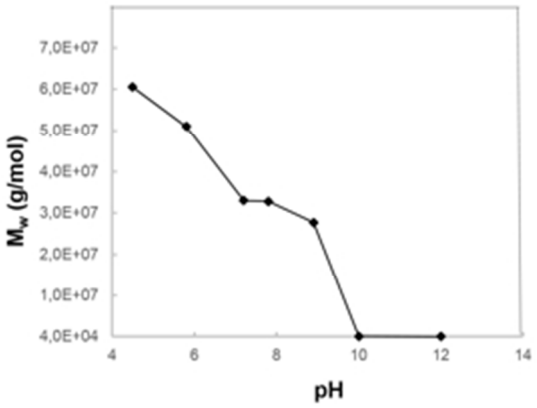

Figure S4: Influence of pH on molecular weigth (Mw) of A45B110C37 copolymers

97x74mm (72 x 72 DPI)

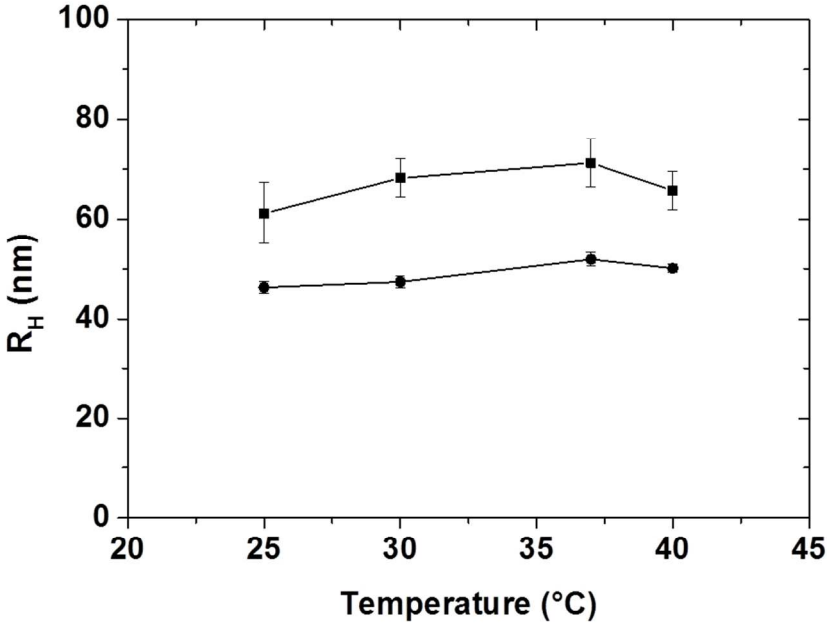

Figure S5. Effect of temperature on particle size of ABC copolymers. (squares) A45B110C37; (circles) A45B101C27.

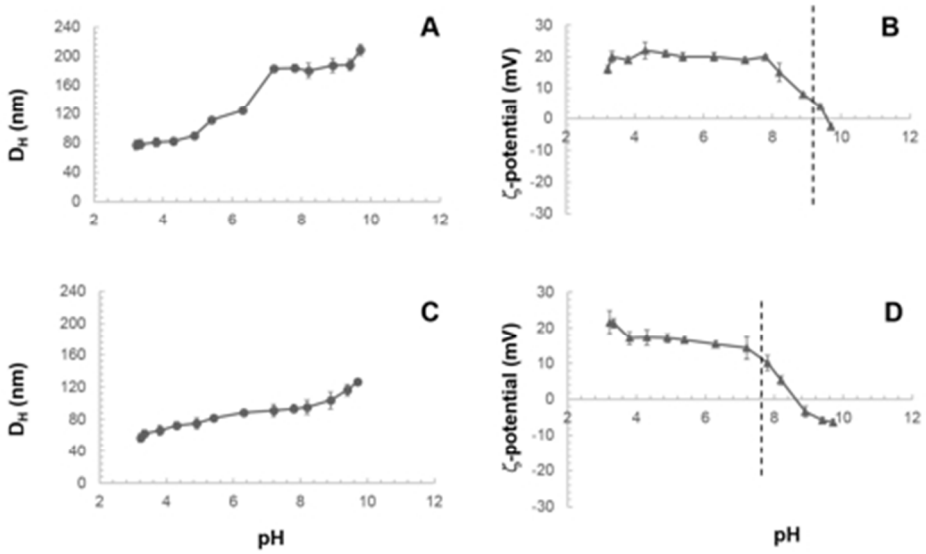

Figure S6. Titration measurements of ABC copolymers: (A) and (B) A45B110C37 Circles: Hydrodynamic diameter (DH) Triangles: -potential. (C) and (D) A45B101C27 Circles: Hydrodynamic diameter (DH) Triangles: -potential. Dash lines: Isoelectric point.

165x100mm (72 x 72 DPI)

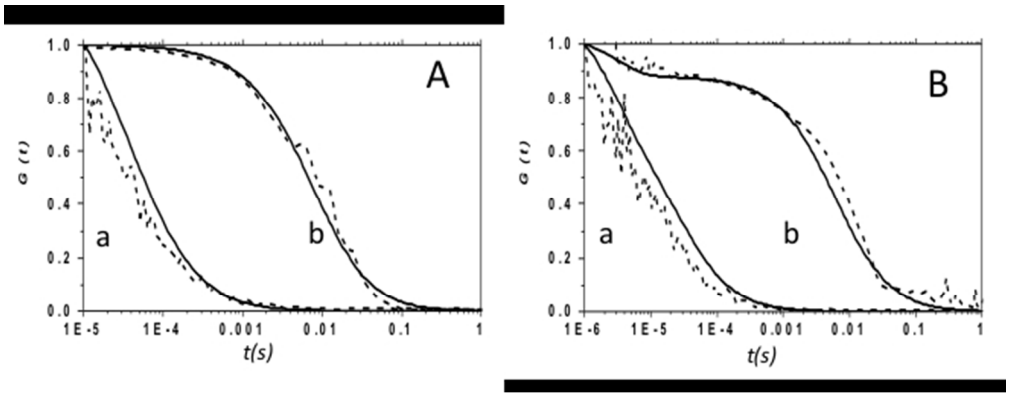

Figure S7. (A) FCS autocorrelation curves (continuous lines) and their fit (dashed lines) of: Free BSA-FITC (a) and BSA-FITC-A45B110C37 (b). (B) BSA-FITC (a) and BSA-FITC A45B101C27 (b). Curves normalized to 1 to facilitate comparison.

232x89mm (72 x 72 DPI)

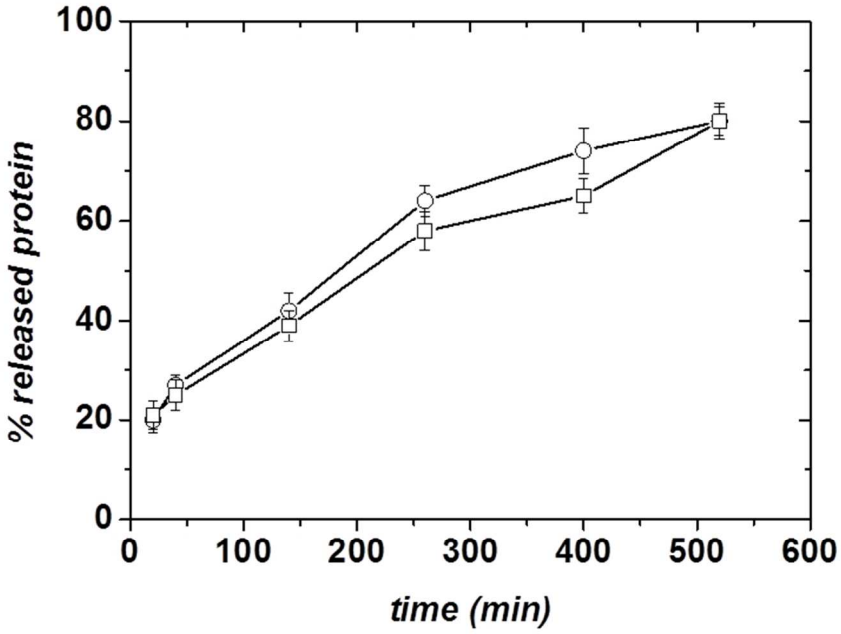

Figure S8. BSA-FITC release from ABC nanoparticles as a function of time at pH = 5.8. (diamonds) A45B31C44; (triangles) A45B84C85; (circles) A45B101C27; (squares) A45B101C20 followed by FCS.

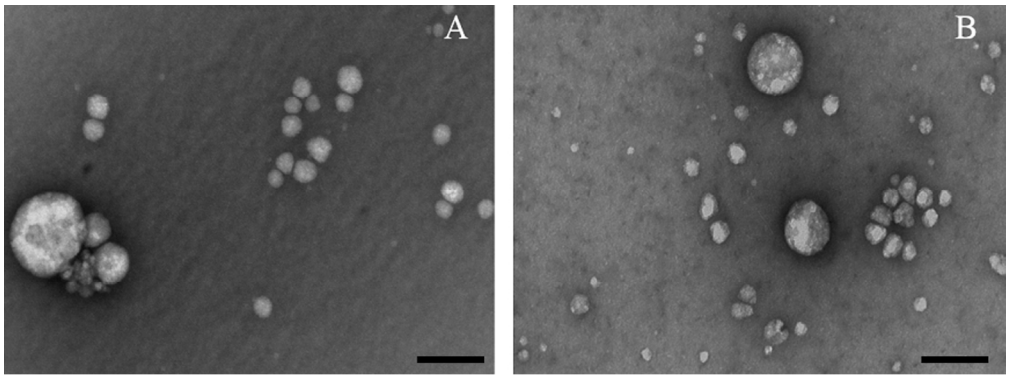

Figure S9. TEM micrographs after attachment of o-ASM to ABC nanoparticles. (A) o-ASM/A45B101C27; (B) o-ASM/A45B110C37. Scale bar: 200 μm. Bright spots are related with the presence of PDMAEMA on the exterion of the nanoparticles. 1-3

228x84mm (150 x 150 DPI)

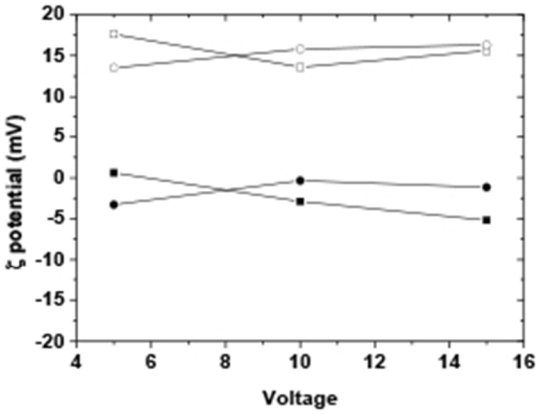

Figure S10. Zeta potential of ABC nanoparticles. (empty squares) A45B110C37 without protein; (empty circles) A45B101C27 without protein; (filled squares) A45B110C37 with protein; (filled circles) A45B101C27 with protein. Protein concentration: 0.058 mg/ml.

115x81mm (72 x 72 DPI)

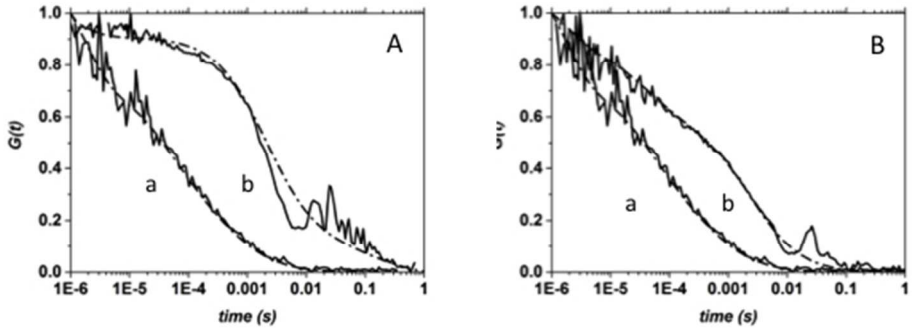

Figure S11. FCS autocorrelation curves (continuous lines) and their fit (dash lines) of: (A) Free o-ASM protein (a), and A45B110C37 nanoparticles attached with non-labelled ASM 50 min after mixing with a solution of free o-ASM (b). (B) free o-ASM (a), and A45B101C27 nanoparticles attached with non labelled ASM 50 min after mixing with a solution of o-ASM (b). Curves normalized to 1 to facilitate comparison.

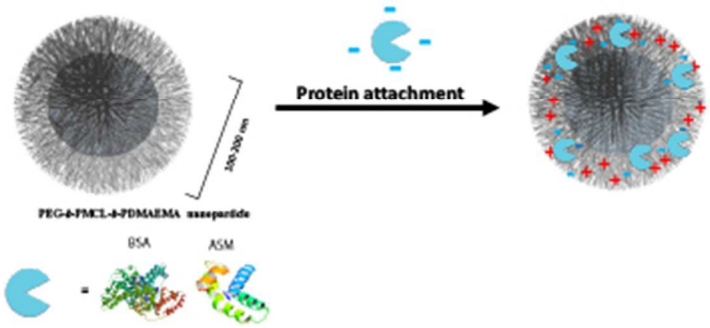

Scheme 1. Schematic illustration of the self-assembly of PEG-b-PMCL-b-PDMAEMA copolymers before and after interaction with a charged protein at pH 7.2.

126x69mm (72 x 72 DPI)